Bol. Soc. Paran. Mat.
©SPM – E-ISSN-2175-1188
SPM: www.spm.uem.br/bspm

(3s.) **v. 2026 (44) 2** : 1–21.
ISSN-0037-8712
doi:10.5269/bspm.81581

Computational and Heat Transfer Analysis of Parabolic Trough Solar Collectors (PTSC) Using Magnetized Hybrid Ree-Eyring Nanofluids with Variable Heat Source

Hamayat Ullah, Zahir Shah, Waris Khan, Maria Alina Fălădău, Aseel Smerat and Rashid Jan

ABSTRACT: Parabolic trough solar collectors (PTSC) are widely used for medium-temperature applications, typically operating within a temperature range of 60–400 °C . These systems primarily serve the purpose of heat and power production. In recent years, solar energy has emerged as a significant source of renewable heat energy. This study explores the enhancement of heat transfer efficiency by employing a hybrid nanofluid composed of graphene oxide and alumina alloy (GO-AA7075), analyzing its non-Newtonian characteristics using the Ree-Eyring fluid model. The study applies the Darcy-Forchheimer condition to evaluate pressure drop due to fluid-solid interactions, while also examining the effects of thermal elevation and velocity slip over a curved surface. This study aims to enhance heat transfer effectiveness in parabolic trough solar collectors by utilizing a hybrid nanofluid comprising graphene oxide and alumina alloy under varying thermal and flow conditions. Using all assumptions on the geometry, the momentum and energy equations are reduced to non-linear partial differential equations. The derived highly coupled and non-linear partial differential equations are non-dimensionalized using dimensionless variables. HAM (Homotopy Analysis Method) is applied to solve the differential equations with the help of Mathematica. The addition of nanoparticles enhanced the thermal conductivity of the fluids, so enhancing the efficiency of heat dissipation. The heat transfer efficiency of the hybrid nanofluid is assessed directly at different concentrations of graphene oxide with alumina alloy, thermal radiation levels, space-dependent heat source, curvature parameters, and flow rates. The Ree-Eyring fluid model precisely predicts the complex flow behavior and heat transfer characteristics, enabling the optimization of operational parameters for improved performance. The finding indicates that the hybrid nanofluid (GO-AA7075) significantly improve heat transfer efficiency. The findings reveal that the graphene oxide combined with alumina alloy in the base fluid is an effective solution for enhancing heat transfer efficiency in various engineering applications. The graphs indicate that for greater values of magnetic parameter the velocity profile declined, while temperature is enhanced.

Keywords: Alumina Alloy (AA7075) hybrid nanofluid, curved surface, graphene oxide, magneto hydrodynamics, thermal radiation.

Contents

2020 *Mathematics Subject Classification:* 76A05.
Submitted January 27, 2026. Published March 14, 2026

Nomenclature:

Symbols	Description	Units
GO-AA7075	Graphene oxide and alumina alloy	–
A	Stretching rate	–
$B(t)$	Magnetic field	–
c_b	Drag constant	–
c_p	Heat capacity	$(J/Kg/K)$
$q_1 = -(4\sigma^*/3K^*)\frac{\partial T^4}{\partial r}$	Rosseland radiative heat flux	–
$q''' = \frac{k_{hnf}u_w}{(\rho c_p)_{hnf}2l\nu}(\Gamma_1(T_w - T_\infty)f' + \Gamma_2(T - T_\infty))$	Variable heat source	–
t	Time	(s)
T	Temperature	(K)
k	Thermal conductivity	$(W\,m^{-1}\,K^{-1})$
K	Absorptivity of permeable medium	–
L_f, L_θ	Linear operators	–
$M = \frac{\sigma_f B_0^2}{A\rho_f}$	Magnetic parameter	–
$Re_s = \frac{u_w l}{\nu_f}$	Local Reynolds number	–
Rd	Radiation parameter	–
Nu_s	Local Nusselt number	–
$Pr = \frac{\nu_f}{\alpha_f}$	Prandtl number	–
Re_x, Re_y	Local Reynolds numbers	–
k	Thermal conductivity	–
C_{fs}	Skin friction	–
f, g	Momentum function (Dimensionless)	–
u, v, w	Velocities along x, y, z ? axis	$(m\,s^{-1})$
u_w	Stretching velocity	$(m\,s^{-1})$
w_w	Mass flux velocities	–
(r, s)	Curvilinear coordinates system	(m)
Greek symbols are given below		
Γ_1, Γ_2	Space and temperature-dependent factors	–
α	fluid parameter	–
α_1	Special symbol for Ree-Eyring fluid model parameter	–
α_f	Thermal diffusivity of the base fluid	–
θ	Dimensionless temperature function	–
η	Dimensionless variable	–
ρ	Density	$(kg\,m^{-3})$
μ	Dynamic viscosity	$(kg\,m^{-1}\,s^{-1})$
ν	Kinematic viscosity	$(m^2\,s^{-1})$
τ	Dimensionless time variable	–
ϕ	Nanoparticle volume fraction	–
σ	Electrical diffusivity of fluid	$(m^2\,V^{-1}\,s^{-1})$
σ^*	Stefan?Boltzmann constant	–
Subscripts:		
hnf	Hybrid Nano-fluid	–
nf	Nano-fluid	–
f	Base fluid	–

1. Introduction

Currently, Hybrid nanofluids, which are composed of nanoparticles consistently dispersed in conventional heat transfer fluids, have attracted significant attention due to their superior thermal properties. Hybrid nanofluids based on graphene oxide is one of the most advantageous for efficient heat transfer applications, as recent studies demonstrate that using graphene oxide nanoparticles into traditional heat transfer fluids can greatly enhance their thermal conduction and heat transfer ability. F. Mebarek-Oudina et al. [1] investigated how geometric parameters affected free convective heat transfer in a hollow with zigzag walls that contained a hybrid nano-fluid made of water-suspended single-walled carbon nanotubes (SWCNT) and magnesium oxide (MgO). The flow of a conductive liquid over a curved surface leads to interactions with an external magnetic field and induces electric currents within the fluid and generating

MHD effects. In order to better understand the impacts of internal heat generation and absorption, F. Mebarek-Oudina et al. [2] examined the flow dynamics of magnetohydrodynamic Burgers' fluid caused by a stretching cylinder. The flow of tangent hyperbolic MHD nanoliquids along a non-isothermal, coagulated stretched sheet under convective heat and mass-convective boundary conditions was investigated by K.V. Prasad et al. [3]. They investigated the combined effects on velocity and temperature profiles of varied thermal conductivity, variable viscosity, thermophoresis, Brownian motion, wall thickness, and Biot number. The curvature parameter is important in heat transfer properties because it affects the velocity fields and thermal transport mechanisms near the curved surface. Surface curvature influences the velocity distribution and flow behavior, thereby affecting the heat transfer characteristics and this concept of heat transfer governed by space-dependent parameters underscores the influence of geometric variations [4]. A steady mixed convection in a two-dimensional enclosure filled with nanoliquid Cu/H_2O through a porous material was numerically investigated by B. Ould Said et al [5]. They observed that as the Reynolds number (Re) increases, heat transport also increases noticeably. The highest heat transmission occurs for the location conditions L = 0.25, Re = 50, and Gr = 105. Casson nanofluid over a stretched surface with activation energy was studied by Jawad Raza et al [6]. They concluded that δ should be maximized for any Nb and Nt to improve heat transfer and showed that temperature and heat transfer rate increased with increases in many parameters such as Ha,Nr,Nb, and Nt but decreased with λ. M. Anil Kumar et al. [7] investigated how radiation, Soret, and Dufour affected the laminar flow of a rotating fluid across a permeable plate while a chemical reaction was taking place. The results of this study showed that while increases in the thermal radiation factor resulted in commensurate increases in the temperature distribution, increases in the Soret and Dufour parameters raised velocity profiles.

A solar collector converts sunlight into usable heat or electrical energy, and the performance of solar collectors can be enhanced through the integration of hybrid nanofluids. These advanced fluids, when used in solar collectors, contribute to more efficient thermal energy absorption and transfer, ultimately improving overall system efficiency. The inherent stability and suspension attributes of HNF are central in improving challenges such as deposit and blocking within solar collectors and these properties preserve continuous performance and maximized the long-term efficiency of solar thermal systems [8]. PTSC are utilized in concentrating solar power systems, using a parabolic-shaped reflector that converges solar radiation onto a receiver aligned along the focal axis of the trough, which enhances thermal energy collection by directing focused solar flux onto a slim receiver [9]. A heat transfer fluid inside the receiving tube captures the concentrated solar energy and transfers it to a heat exchanger, in which thermal energy is transformed into another kind of energy [10], and the influence of irregular heat thermal on a cross nanofluid has been investigated by Aziz et al [11]. According to this study, increasing the absorption and flow circumstances of nanoparticles may result in enhanced thermal performance and decreased entropy formation. Rashid et al [12] examined an extended sheet in the presence of an energy source and the influence of how well the system can transfer heat, offering opportunities to improve its efficiency. A theoretical study on nanofluids influence on natural convection in uneven solar collectors was projected by Kadri et al [13], where the potential for significant enhancements in heat transfer and overall efficiency due to the combined effects of nanoparticle-enhanced thermal properties and the unique flow dynamics, convinced by the curvy surfaces, is emphasized. Alnaqi et al. [14] analyzed the effectiveness of PDSC of an oil-based filled cross nanoliquid, and Ahmad et al [15] did a theoretical analysis of the thermal performance of a cross nanoliquid filled with nanoparticles. A nanoparticle solution with a greater heat transmission range than conventional fluids is examined by Choi et al [16]. The effectiveness of TiO_2/H_2O nano liquid in flat solar collectors was examined experimentally by Chaji et al [17]. Ghasemi and Ahangar [18] quantitatively investigated the performance of Cu/H_2O nanofluid on parabolic solar collectors (PSCs). The possible means of available energy to be utilized in the flow environment must also be studied as part of the best thermally effective fluid under different circumstances. It should either be consumed or stored for other purposes. Khodabandeh [19] attempted to manage the energy in a heated cylindrical duct. Later on, Liu et al [20] employed a solar warming design to examine energy. Jamshed et al [21] worked to enhance heat transfer efficiency, the evaluation encompassed fine-tuning diverse parameters, including fluid concentration, flow rate, and temperature gradients. The findings delivered directives for attaining optimal operational states in PTSCs. Mahmood et al [22] did an investigation to examine the thermal efficiency of solar collectors.

Many applications necessitate non-Newtonian, where shear rates and shear stresses are interconnected in a non-linear manner. The duration of the shear stress significantly affects the shear rate. Consequently, factors such as viscosity do not adequately describe shear stress in these nanofluids. As a result, several mathematicians have discussed the class of non-Newtonian models, one of which is the Ree-Eyring model. In this context, Hayat et al [23] examined the entropy in the flow and also Puneeth conduct a theoretical investigation into the thermal properties of nanofluid as it flows past a stretching sheet influenced by bioconvection [24]. They found that the combination of bioconvection and the non-Newtonian behavior of Ree-Eyring nanofluids significantly enhances heat transfer in the flow past a stretching sheet, optimizing thermal performance under specific conditions.

The novelty of current work is to analyze the flow dynamics of Ree-Eyring fluid with water-based GO and AA7075 hybrid nanofluid, with a focus on heat transfer enhancement. Nonlinear thermal radiation is used to study heat transmission behaviors, heat exchange and other Brownian motion properties. HAM is used to derive solutions for the resulting nonlinear similarity equations and numerical findings are subsequently shown graphically for a variety of parameter values. This study observes the behavior of a hydromagnetic water-based graphene oxide hybrid nanofluid with an alumina alloy on curved surfaces by employing the Ree-Eyring fluid model. This combination hasn't been studied before in this model framework. To examine the temperature variation that occurs in space, the space-dependent heat source/sink and thermal radiation are illustrated. Numerical simulations are used in the research to provide more reliable and robust results and to give a thorough understanding of the mechanisms boosting the transmission of heat in the hybrid nanofluid.

2. Formulation and Geometry of the Problem

In this study, we investigated a two-dimensional, steady boundary layer flow of water-based magnetized hybrid nanofluids comprising graphene oxide (GO) and a combination of GO with AA7075 nanoparticles, over a curved surface, within the framework of the Ree?Eyring fluid model. A curvilinear coordinate system (r,s) is employed, where r represents the radial direction and s denotes the arc length along the surface. The surface stretching velocity in the s-direction is defined as $u_w = Ae^{s/l}$, where A $>$ 0 and l $>$ 0 correspond to the stretching rate and characteristic length, respectively. The direction r is orthogonal to the tangential direction ss, as illustrated in Figure 1. A transverse magnetic field B(t) is applied Normal to the surface. The analysis incorporates the influences of heat generation, Joule heating, and spatially variable thermal conductivity. The physical configuration of the problem, including the coordinate framework and velocity components, is depicted in Figure 1.

2.1. Assumptions of the model

- Two-dimensional steady boundary layer flow of water-based magnetized hybrid nanofluids flow
- Graphene oxide (GO) and GO+AA7075 nanoparticles
- Curved surface
- Ree-Eyring fluid model
- The effects of heat generation, Joule heating, and variable thermal conductivity

The basic governing equations for the fluid motion and heat transfer are

$$\nabla \cdot \mathbf{V} = 0, \tag{1}$$

$$\rho_{hnf}\left(\frac{\partial \mathbf{V}}{\partial t} + \mathbf{V}\cdot\nabla\mathbf{V}\right) = -\nabla p + \nabla^2\mathbf{V} + \mathbf{J}\times\mathbf{B}, \tag{2}$$

$$\rho_{hnf}c_{hnf}\left(\frac{\partial T}{\partial t} + \mathbf{V}\cdot\nabla T\right) = k_{hnf}\nabla^2 T. \tag{3}$$

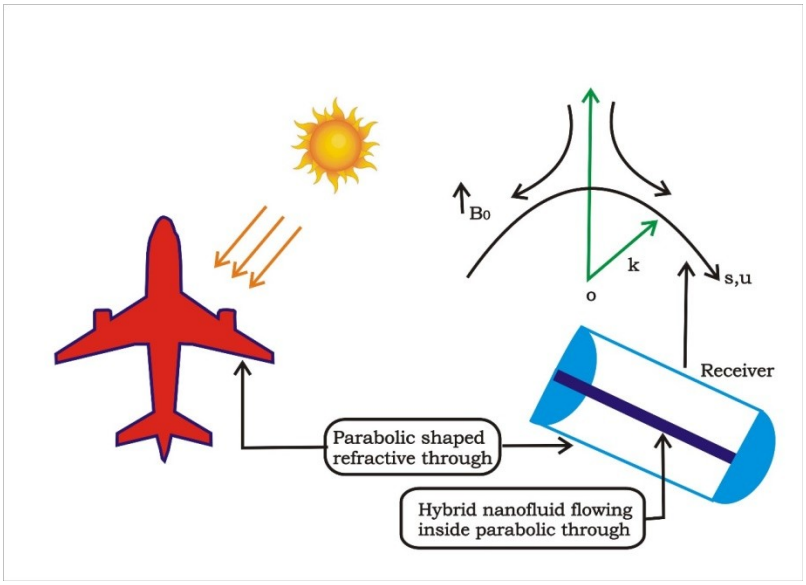

Figure 1: The flow setup and coordinate system.

2.2. Governing Equations After Applying the Assumptions

The following leading equations are based on the previously stated assumptions [25-26].

$$\frac{\partial}{\partial r}\left((r+K)v\right)+K\frac{\partial u}{\partial s}=0, \tag{4}$$

$$\frac{\partial p}{\partial r}-\frac{\rho_{hnf}}{r+K}u^2=0, \tag{5}$$

$$\begin{aligned} v\frac{\partial u}{\partial r}+\frac{vu}{r+K}+\frac{K}{r+K}u\frac{\partial u}{\partial s}=&-\frac{1}{\rho_{hnf}(r+K)}\frac{\partial p}{\partial s}+\frac{1}{\rho_{hnf}}\left(\mu_{hnf}+\frac{1}{B_{c1}}\right)\left[\frac{\partial^2 u}{\partial r^2}+\frac{1}{r+K}\frac{\partial u}{\partial r}-\frac{1}{(r+K)^2}u\right]\\ &-\frac{1}{\rho_{hnf}}\frac{\mu_{hnf}}{k_0}u-\frac{1}{\rho_{hnf}}\frac{c_b}{\sqrt{k_0}}u^2-\frac{\sigma_{hnf}B_0^2}{\rho_{hnf}}u, \end{aligned} \tag{6}$$

$$\begin{aligned} v\frac{\partial T}{\partial r}+\frac{Ku}{r+K}\frac{\partial T}{\partial s}=&\alpha_{hnf}\left(\frac{\partial^2 T}{\partial r^2}+\frac{1}{r+K}\frac{\partial T}{\partial r}\right)+\frac{q'''}{(\rho c_p)_{hnf}}-\frac{1}{(r+K)(\rho c_p)_{hnf}}\frac{\partial}{\partial r}\left[(r+K)q_1\right]\\ &+\frac{1}{(\rho c_p)_{hnf}}\left(\mu_{hnf}+\frac{1}{B_{c1}}\right)\left(\frac{\partial u}{\partial r}\right)^2, \end{aligned} \tag{7}$$

Governed by the following boundary conditions [27]:

$$\begin{aligned} &u=u_w=Ae^{\frac{s}{l}},\quad v=0,\quad -K_{hnf}\frac{\partial T}{\partial r}=h_f(T_w-T)\quad \text{at}\quad r=0,\\ &u\to 0,\quad \frac{\partial u}{\partial r}\to 0,\quad T\to T_\infty,\quad \text{at}\quad r\to\infty. \end{aligned} \tag{8}$$

Table 1: Description of the model

Description	**Mathematical Expression/Definition**
Velocity components	u and v represent the velocity components in the s- and r-directions, respectively.
Drag constant	c_b denotes the drag coefficient associated with the resistance in the porous medium.
Absorptivity of the permeable medium	κ is the measure of the medium's ability to absorb radiation energy.
Rosseland radiative heat flux	$q_1 = -\left(\frac{4\sigma^*}{3K^*}\right)\frac{\partial T^4}{\partial r}$
Variable heat source	$q''' = \frac{k_{hnf}u_w}{(\rho c_p)_{hnf}2lv}\left(\Gamma_1(T_w - T_\infty)f' + \Gamma_2(T - T_\infty)\right)$ (9)

Here Γ_1 and Γ_2 are space and temperature-dependent factors.

2.3. Transformations

Similarity transformations are [9]:

$$\xi = \left(\frac{Ae^{\frac{s}{l}}}{2\nu_f l}\right)^{0.5} r, \quad u = Ae^{\frac{s}{l}}f'(\xi), \quad v = -\left(\frac{A\nu_f e^{\frac{s}{l}}}{2l}\right)^{2.5}\frac{\kappa}{r+\kappa}\left(f(\xi) + \xi f'(\xi)\right),$$
$$p = p_f A^2 e^{\frac{s}{l}} p(\xi), \quad T - T_\infty = \theta(\xi)(T_w - T_\infty) \tag{10}$$

Utilizing the above dimensionless quantities, the continuity equation is satisfied. After eliminating pressure by using cross-differentiation, the governing equations (1)-(5) can be expressed as follows:

$$P' - \frac{\rho_{hnf}}{\rho_f}\left(\frac{1}{\xi+\gamma}\right)f'^2 = 0 \tag{11}$$

$$\left(\frac{\mu_{hnf}}{\mu_f} + \alpha_1\right)\left(f''' + \frac{f''}{\xi+\gamma} + \frac{f}{(\xi+\gamma)^2}\right) - \left(\frac{\rho_{hnf}}{\rho_f}\right)\left(\frac{\xi+2\gamma}{(\xi+\gamma)^2}ff'' - \frac{\gamma}{\xi+\gamma}ff'' - \frac{\gamma}{(\xi+\gamma)^2}ff' - \frac{1}{\xi+\gamma)^2}f'^2\right)$$
$$- M\left(\frac{\sigma_{hnf}}{\sigma_f}\right)\left(f'' + \frac{1}{\xi+\gamma}f'\right) - (4p + \xi p') - \beta_0\left(\frac{\mu_{hnf}}{\mu_f}\right)\left(f'' + \frac{1}{\xi+\gamma}f'\right) - Fr\left(f'' + \frac{1}{\xi+\gamma}f'\right)^2 = 0 \tag{12}$$

$$\left(\frac{k_{hnf}}{k_f} + Nr\right)\left(\theta'' + \frac{1}{\xi+\gamma}\theta'\right) + Pr\left(\frac{(\rho C_p)_{hnf}}{(\rho C_p)_f}\frac{\gamma}{\xi+\gamma}(f\theta' - f'\theta) + (\Gamma_1 f' + \Gamma_2\theta)\right)$$
$$+ \left(\frac{\mu_{hnf}}{\mu_f} + \alpha_1\right)Pr\,Ec\,(f'')^2 = 0 \tag{13}$$

By eliminating pressure from Eqs. (11) - (13), we obtain the following transformed form:

$$\left(\frac{\mu_{hnf}}{\mu_f} + \alpha_1\right)\left(f'''' + \frac{2f'''}{\xi+\gamma} + \frac{f'}{(\xi+\gamma)^3} - \frac{f''}{(\xi+\gamma)^2}\right) - 2Fr\left(2f'f'' + \frac{1}{\xi+\gamma}f'^2\right) + \left(\frac{\rho_{hnf}}{\rho_f}\right)$$
$$\left(\frac{\gamma}{(\xi+\gamma)^2}ff'' + \frac{\gamma}{\xi+\gamma}ff''' - \frac{\gamma}{(\xi+\gamma)^3}ff' - \frac{3\gamma}{(\xi+\gamma)^2}f'^2 - \frac{3\gamma}{\xi+\gamma}f'f''\right) \tag{14}$$
$$- M\left(\frac{\sigma_{hnf}}{\sigma_f}\right)\left(f'' + \frac{1}{\xi+\gamma}f'\right) - \beta_0\frac{\mu_{hnf}}{\mu_f}\left(f'' + \frac{1}{\xi+\gamma}f'\right) = 0$$

Subject to boundary conditions

$$f'(\xi) = 1, \quad f = 0, \quad \theta'(\xi) = Bi(\theta - 1), \quad \text{when } \xi = 0,$$

$$f'(\xi) \to 0, \quad f''(\xi) \to 0, \quad \theta \to 0, \quad \text{when } \xi \to \infty. \tag{15}$$

Table 2: Models Parameters

Name of Parameter	**Symbol & Formula**
Curvature parameter	$\gamma = K\left(\frac{Ae^{s/l}}{2\nu_f}\right)^{0.5}$
Thermal radiation	$Nr = \frac{16\,\sigma^*\,T^3}{3k_f\,k^*}$
Forchheimer number	$Fr = \frac{SC_b}{k_0^{1/2}}$
Wall friction	$Re_s^{1/2}C_{fs} = \frac{1}{(1-\beta_1)(1-\beta_2)^{2.5}}\left(f''(0) - \gamma f'(0)\right)$
Ree-Eyring fluid model parameter	$\alpha_1 = \frac{1}{\mu_f BC_1}$
Magnetic field	$M = \frac{\sigma_f B_0^2}{A\rho_f}$
Prandtl number	$Pr = \frac{\nu_f}{\alpha_f}$
Local Nusselt number	$Re_s^{-1/2}Nu_s = -\left(\frac{k_{hnf}}{k_f} + Nr\right)\theta'(0)$
Biot number	$Bi = h_f\left(\frac{2\nu_f l}{Ae^{s/l}}\right)^{0.5}$
Local Reynolds number	$Re_s = \frac{\mu_w l}{\nu_f}$

3. Thermo-Physical Properties of Fluids Used

The thermo-physical appearances and relation of nano and hybrid nanofluid are exposed in Tables 2 & 3 respectively. Assets and applications of the considerable hybrid nanofluids are shown in Figure 2 (a, b) respectively.

Table 3: A Previous study [15] has analyzed and reported in great detail the thermophysical properties of the base fluid and the HNF.

Properties constituents	c_p (J/kgK)	k (W/mK)	$\sigma\ \left(\frac{\mathrm{S}}{\mathrm{m}}\right)$	ρ (kg/m^3)
Graphene oxide (GO)	3600.0	3000.0	4.57×10^{-6}	3600.0
$AA7075$	862.0	121.61	434.81	2810.0
H_2O	4179.0	0.6130	0.005	997.10

Table 4: Nanofluids and hybrid nanofluids thermo-physical connections [9].

Properties	**Nano and Hybrid**
Dynamic viscosity	$\mu_{hnf} = \frac{\mu_f}{(1-\beta_1)^{2.5}(1-\beta_2)^{2.5}}$
Heat Capacitance	$(\rho C_p)_{hnf} = \left[(1-\beta_2)\left[(1-\beta_1) + \frac{\beta_1(\rho C_p)_{1s}}{\rho_f}\right] + \frac{\beta_2(\rho C_p)_{2s}}{(\rho C_p)_f}\right](\rho C_p)_f$
Thermal Conductivity	$k_{hnf} = \frac{2\beta_1 k_{1s} + k_{1s} + 2k_f - 2\beta_1 k_f}{k_{1s} + 2k_f + \beta_1(k_f - k_{1s})}$ Here k_{1s} is the thermal conductivity of the first solid phase and k_f is the thermal conductivity of the base fluid.
Electrical conductivity [9]	$\sigma_{hnf} = \sigma_f\left[1 + \frac{3\sigma_{1s}\beta_{1s} + \beta_{2s}\sigma_{2s} - 3(\beta_1+\beta_2)\sigma_f}{\sigma_{1s}(1-\beta_{1s}) + (2+\beta)\sigma_f + \sigma_{2s}(1-\beta_{2s})}\right]$

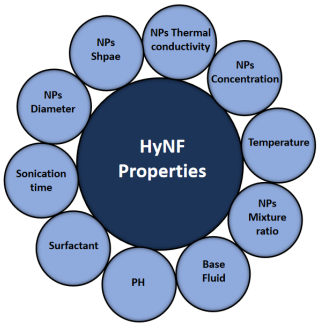

(a) Features inducing the hybrid nanofluids properties.

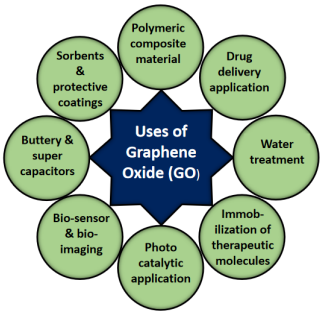

(b) Schematic for applications of Graphene Oxide (GO) Nanoparticles

Figure 2: Hybrid nanofluids: structure and applications.

4. Quantities (Physical) of Engineering Interests

Table 5: The physical quantities of interest in the current work are:

Definition	Dimensional Form	Non-Dimensional Form	
Skin friction coefficient	$C_{fs} = \frac{\tau_w}{\rho_f u_w^2}$	$C_f(Re_s)^{1/2} = \left(\frac{\mu_{hnf}}{\mu_f} + \alpha_1\right)\left(f''(0) + \frac{f'(0)}{\xi+\gamma}\right)$	(16)
Nusselt number	$Nu_s = \frac{sq_w}{k_f(T_w - T_\infty)}$	$Nu_s(Re_s)^{-1/2} = -\theta'(0)$	(17)

Table 6: Non-dimensional form

Description	Expression	
Surface shear stress	$\tau_{rs} = \left[\left(\mu_{hnf} + \frac{1}{Bc_1}\right)\left(\frac{\partial u}{\partial r} + \frac{u}{r+K}\right)\right]_{r=R}$	(18)
Surface heat flux	$q_w = -k_{nf}\left[\frac{\partial T}{\partial r}\right]_{r=0}$	
Local Reynolds number	$Re_s = \frac{u_w l}{\nu_f}$	

5. Solution Methodology

Due to the nonlinearity and coupling in Equations (10) and (11), it is not possible to solve the problem in a closed form. Consequently, HAM is employed to numerically solve the system of Equations in the above section. The solutions having auxiliary parameters h adjust and control the convergence of the solutions. Homotopy Analysis Method is one of the powerful analytical techniques. HAM propositions flexibility and exactness for solving such types of nonlinear problems without relying on small parameters. Yet, its efficiency depends upon the selection of appropriate parameters. It?s computationally challenging for complex systems. Another drawback, HAM remains a valuable tool in mathematical modeling, especially in engineering and physics. The starting guess functions are

$$f_0(\hat{i}) = 1 - e^{-\hat{i}}, \quad \theta_0(\hat{i}) = \frac{Bi}{1+Bi}e^{-\hat{i}} \tag{19}$$

L_θ, L_f are linear operators and are expressed as:

$$L_f(f) = \frac{d^4 f}{d\hat{i}^4} - \frac{d^2 f}{d\hat{i}^2}, \quad L_\theta(\theta) = \frac{d^2\theta}{d\hat{i}^2} - \theta \tag{20}$$

Which have the following properties:

$$L_f\left(c_1 + c_2 e^{-\hat{i}} + c_3 e^{\hat{i}}\right) = 0, \quad L_\theta\left(c_4 e^{-\hat{i}} + c_5 e^{\hat{i}}\right) = 0 \tag{21}$$

The general solution?s constants are $c_i, i = 1 - 5$.

5.1. Convergence of the solution

Figure 3 represents the h-curve for velocity and temperature profiles. As the series solutions is computed here for the velocity and temperature distribution by employing HAM, the assisting parameters h_f, h_θ appears which control the solution process and are responsible to adjust the convergences.

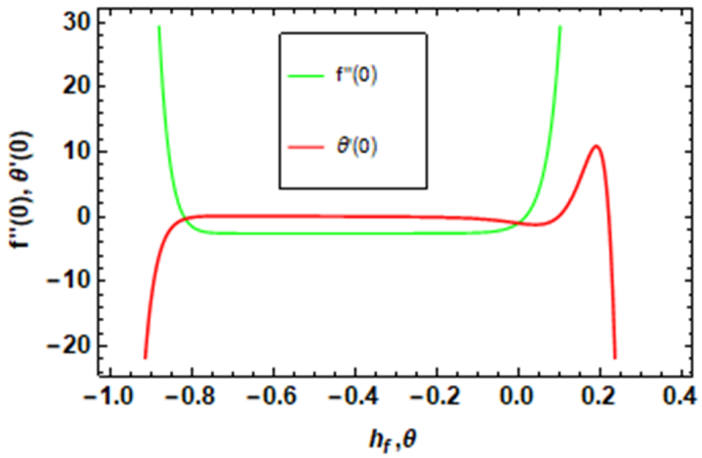

Figure 3: The h-curves for velocity and temperature.

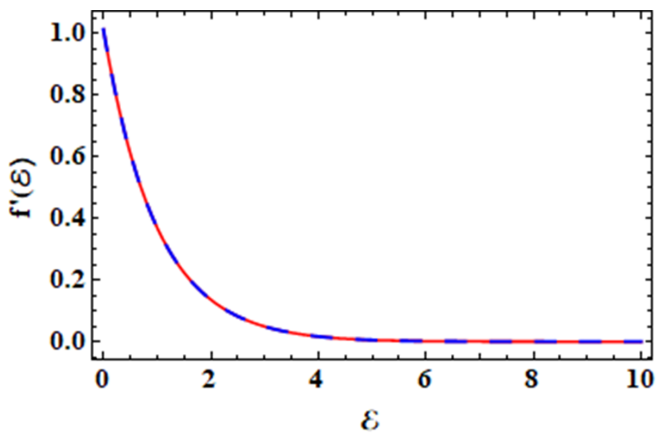

Figure 4: HAM vs numerical method for velocity field.

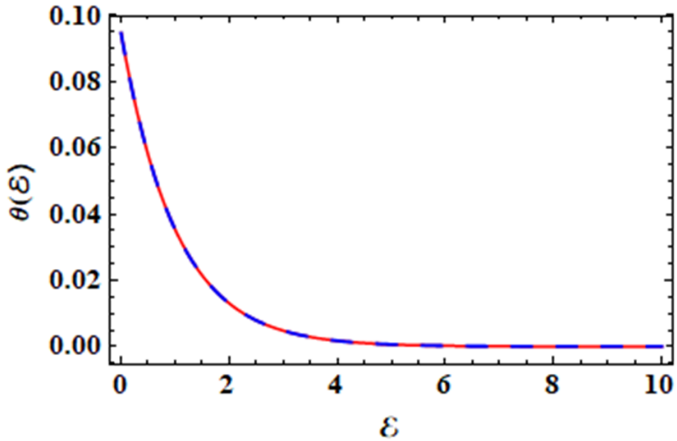

Figure 5: Comparison graph for HAM and numerical method for temperature field.

To obtain the valid region for h-curve of h_f, h_θ for velocity and temperature solutions. From figure 3, the range of h curve for temperature and velocity is valid range. Figures 7, 8 and tables 7, 8 illustrate a comparison of results for both the HAM and numerical technique. Both solutions show close agreement.

Table 7: Comparison results of the Homotopy analysis method and numerical solution for $f(\xi)$.

ξ	HAM results $f(\xi)$	Numerical results $f(\xi)$	Absolute Error
0	1.013090	1.013100	0.000099
1	0.369435	0.369453	0.000620
2	0.135811	0.135811	0.000012
3	0.048973	0.048964	0.000292
4	0.016573	0.016566	0.000240
5	0.005091	0.005087	0.000130
6	0.001388	0.001386	0.000058
7	0.000325	0.000324	0.000024
8	0.000059	0.000058	9.340550×10^{-6}
9	3.771040×10^{-6}	3.664800×10^{-6}	3.541420×10^{-6}
10	-3.368320×10^{-6}	-3.408010×10^{-6}	1.322950×10^{-6}

Table 8: Comparison results of HAM and numerical solution for $\theta(\xi)$.

ξ	HAM Solution $\theta(\xi)$	Numerical Solution $\theta(\xi)$	Absolute Error
0	0.049679	0.094663	0.000523
1	0.035348	0.035340	0.000263
2	0.013067	0.013064	0.000106
3	0.004815	0.004814	0.000040
4	0.001773	0.001772	0.000015
5	0.000652	0.000652	5.554790×10^{-6}
6	0.000240	0.000240	2.046690×10^{-6}
7	0.000088	0.000088	7.533690×10^{-7}
8	0.000032	0.000032	2.772080×10^{-7}
9	0.000012	0.000012	1.019870×10^{-7}
10	4.395650×10^{-6}	4.394530×10^{-6}	3.752000×10^{-8}

6. Results and Discussions

In this investigation, HAM is used to explore the efficiency of various governing factors including the curvature parameter γ, thermal radiation factor Nr, fluid parameter α, the non-dimensional Biot number Bi, the magnetic parameter M, the non-dimensional Forchheimer number Fr, the space-dependent parameter Γ_1 and temperature dependent parameter Γ_2 on the velocity $f^{'}(\xi)$ and temperature $\theta(\xi)$, through graphs.

6.1. Velocity profile

Fig. 6 illustrates the variation in the velocity profile as influenced by M the magnetic parameter. As the magnetic parameter M increases, the velocity profile decreases for the hybrid nanofluid (HNF). A Lorentz force is created when the motion of the fluid interacts with the magnetic field. This force acts in the opposite direction of the fluid motion. Through Joule dissipation, this force acts as a resistive drag, transforming some of the fluid's kinetic energy into heat. Consequently, the fluid encounters increased flow resistance, which lowers its velocity. Consequently, $f^{'}(\xi)$ declines, demonstrating a more significant impact on the fluid flow. Fig. 7 illustrates the relationship between the curvature factor γ and the resistance to flow due to increasing viscosity. As the curvature factor γ increases, the $f^{'}(\xi)$ for the hybrid nanofluid also rises. By increasing the curvature parameter, the fluid is forced outward along the curved surface by centrifugal forces, which also decrease geometric resistance to flow. Higher velocity is the result of the fluid motion being accelerated by this combined effect. Increasing the curvature parameter physically enhances the momentum as it expands the boundary's radius relative to the curved surface. Fig. 8 explains the effect of Forchheimer numbers Fr on the $f^{'}(\xi)$. Furthermore, compared to nanoliquid, it is found that hybrid nanofluid is significantly affected by the variation in Fr. This may be due to the fluid-solid interaction altering the pressure, resulting in high fluidic inertia, which resist the velocity. Consequently, the fluid may respond more slowly to variations in the external environment, leading to a decrease in the velocity profile.

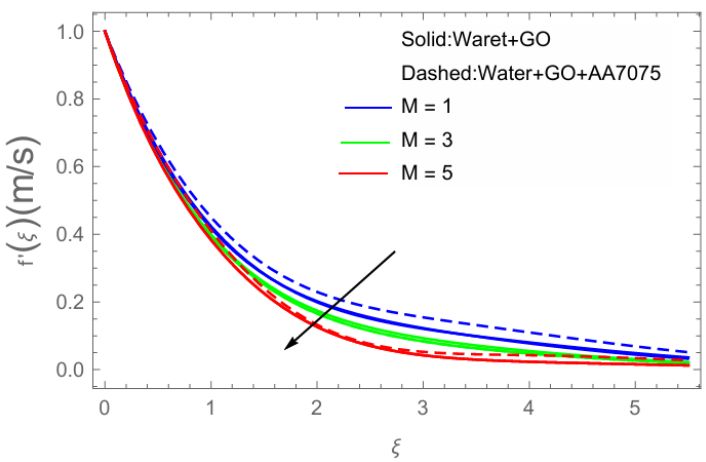

Figure 6: Effect of M (Magnetic parameter) on $f^{'}(\xi)$ (Velocity).

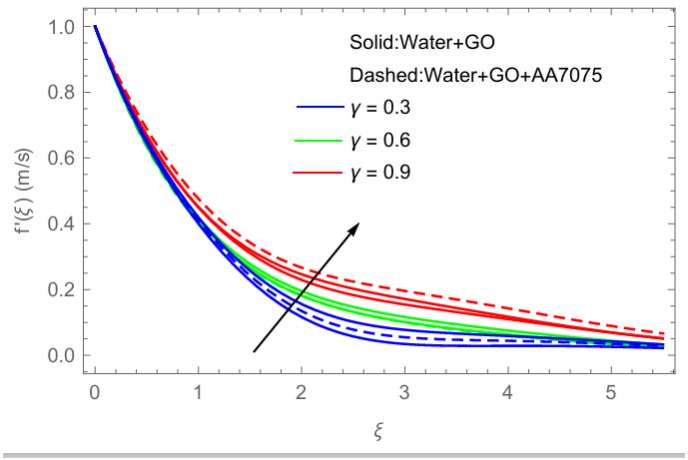

Figure 7: Effect of γ (curvature parameter) on $f^{'}(\xi)$.

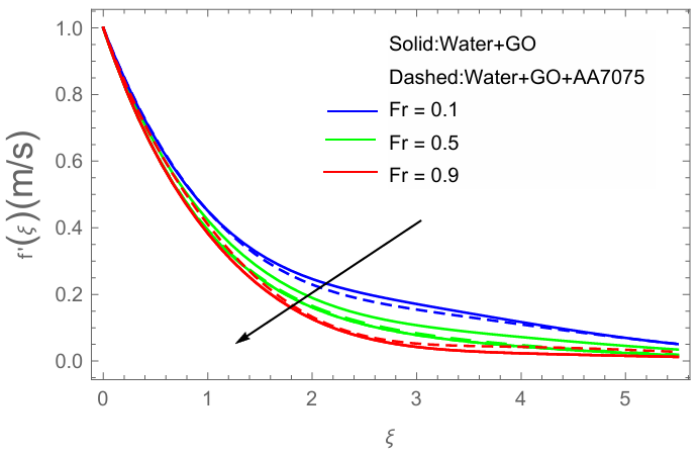

Figure 8: Effect of Fr on $f^{'}(\xi)$.

6.2. Temperature profile:

Figure 9 shows the influence of the magnetic parameter M on the temperature distribution $\theta(\xi)$ and it is observed that an increase in M leads to a corresponding enhancement in the temperature profile of the hybrid nanofluid (HNF). A rise in the magnetic parameter M increases the Lorentz force, which opposes fluid motion and uses Joule heating to transform some of the kinetic energy into thermal energy. The fluid's temperature rises as a result of this energy conversion. Figure 10 explores the variation of the temperature profile $\theta(\xi)$ with respect to the Fr Forchheimer parameter. Higher values of Fr result in an increased temperature profile, because the intensified inertial resistance within the porous medium, which contributes to greater energy dissipation and subsequently elevates the fluid temperature. This suggests that fluid motion plays a more significant role in the overall system energy balance compared to thermal energy changes. The enhanced kinetic energy promotes stronger fluid circulation and mixing, which in turn facilitates more effective convective heat transfer within the fluid medium. Figure 11 highlights the effect of the space-dependent parameter Γ_1 on the temperature distribution $\theta(\xi)$. An increase in Γ_1 leads to a rise in temperature for the hybrid nanofluid (HNF). This can be explained by the increased available space for flow within the porous medium, which enhances fluid motion and convective heat transfer through improved circulation. Figure 12 depicts the variation of the temperature profile $\theta(\xi)$ with respect to the Biot number Bi. It is evident that an increase in Bi leads to higher fluid temperatures.

This trend can be attributed to the greater influence of kinetic energy over enthalpy changes, thereby enhancing thermal energy exchange at the fluid solid interface and elevating the temperature within the hybrid nanofluid. Figure 13 shows the impact of the curvature factor γ on the temperature distribution $\theta(\xi)$. As the curvature factor increases, a decline in the temperature profile is observed. This is due to the increase in surface area per unit volume associated with higher curvature, which enhances heat dissipation from the fluid to its surroundings. The improved cooling effect over the curved surface results in a lower fluid temperature. Figure 14 presents the influence of the time-dependent parameter Γ_2 on the temperature distribution. As Γ_2 increases, the temperature of the HNF also rises. This behavior is a consequence of the increased temporal variation in flow parameters, which intensifies fluid mixing and facilitates a more uniform distribution of thermal energy, thereby raising the overall temperature of the fluid domain. Figure 15 demonstrates the effect of the variable thermal radiation parameter Nr on the temperature profile $\theta(\xi)$ A rise in Nr leads to an increase in temperature, which is linked to the spatial variation in the fluid's thermal conductivity. Enhanced thermal conductivity improves heat transfer across the fluid, resulting in elevated fluid temperatures due to more efficient thermal energy distribution.

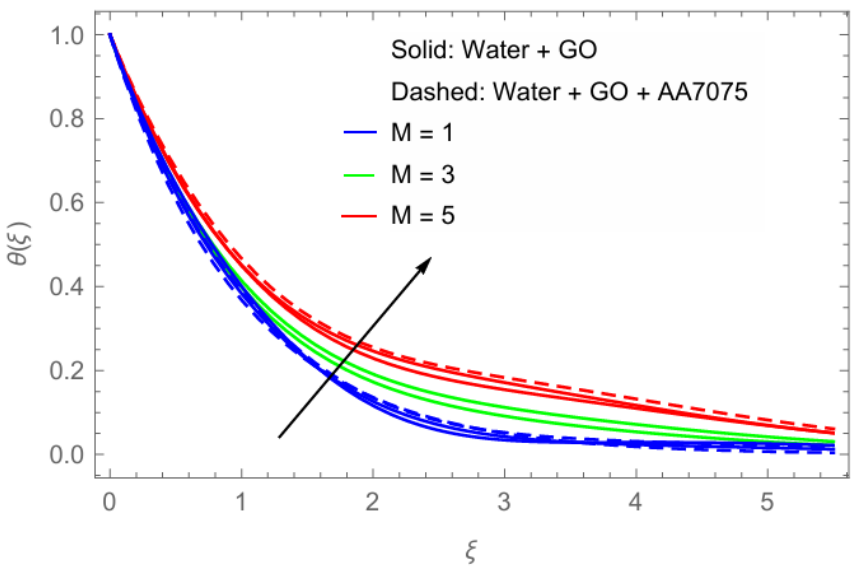

Figure 9: Effect of M on $\theta(\xi)$

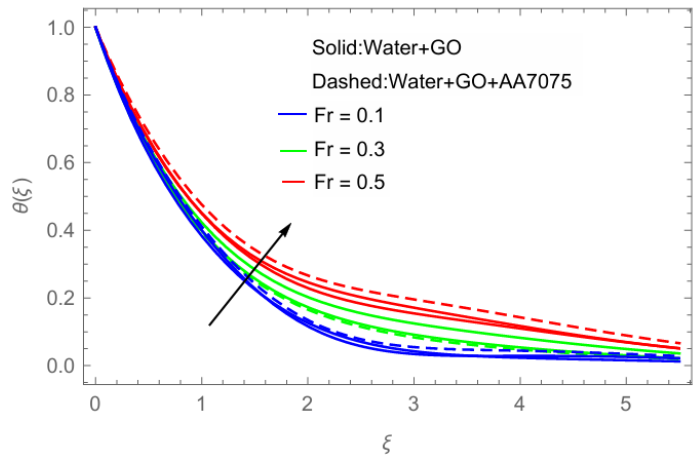

Figure 10: Effect of Fr on $\theta(\xi)$

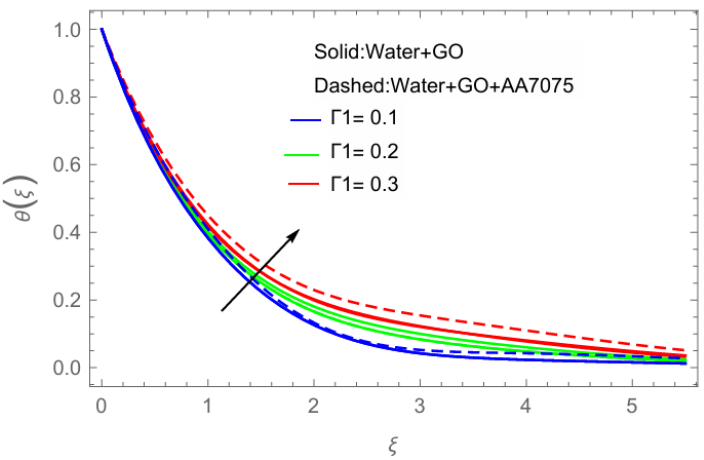

Figure 11: . Effect of Γ_1 on $\theta(\xi)$.

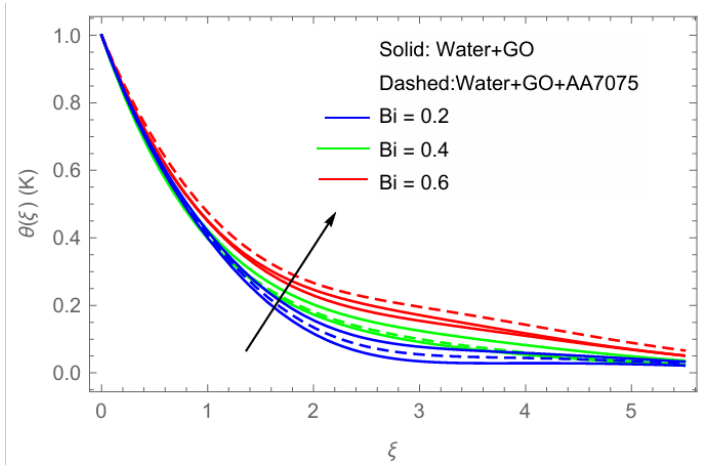

Figure 12: Effect of Bi on $\theta(\xi)$.

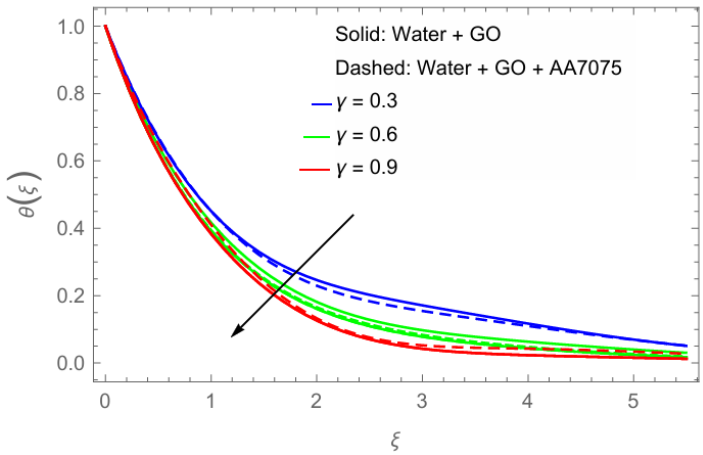

Figure 13: Effect of γ on $\theta(\xi)$.

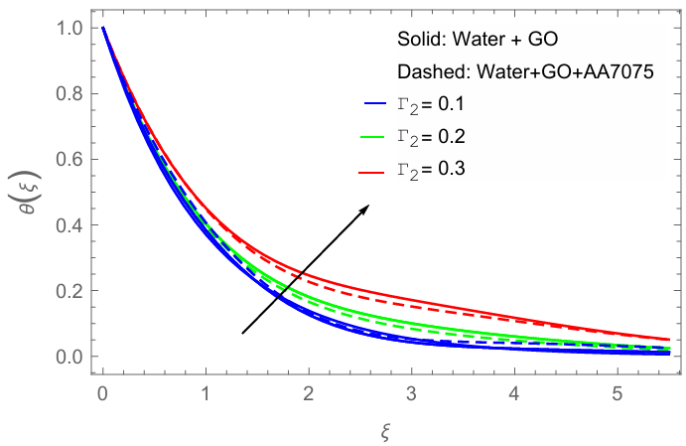

Figure 14: Effect of Γ_2 on $\theta(\xi)$.

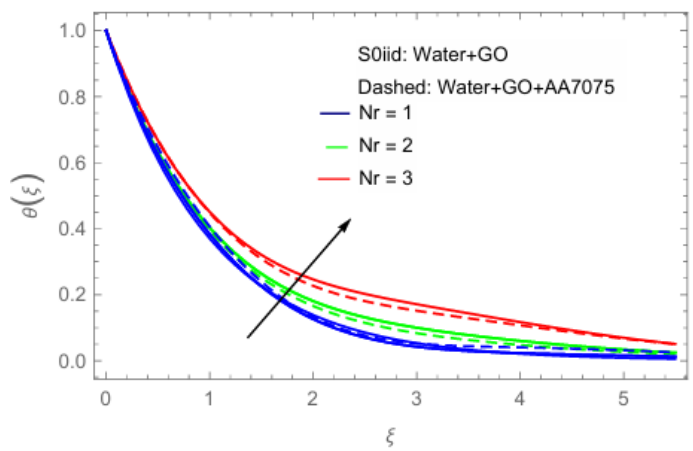

Figure 15: Effect of Nr on $\theta(\xi)$.

6.3. Skin friction and Nusselt number

The impact of M and Fr are shown on skin friction C_{fs} in figure 16 and figure 17. It is clearly observed that the skin friction C_fs increases when the effect of M and Fr are enhanced. The skin friction rises with the MHD nanofluid flow due to the denser Hartmann layer and reduces the velocity gradient closed to the solid surfaces, which in turn enhance the shear stress and the drag force. The same results is observed for Fr. The impact of Ec and Nr are shown on Nu_s in figure 18 and figure 19. The increasing effect is observed for both Ec and Nr are shown on Nu_s.

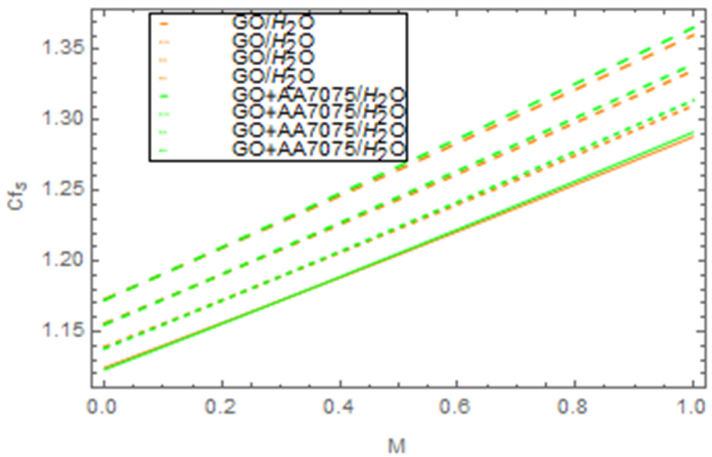

Figure 16: Effect of M on C_{fs}.

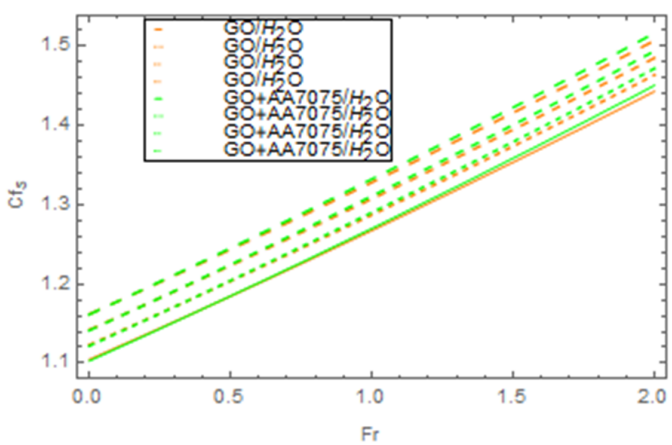

Figure 17: Effect of Fr on C_{fs}.

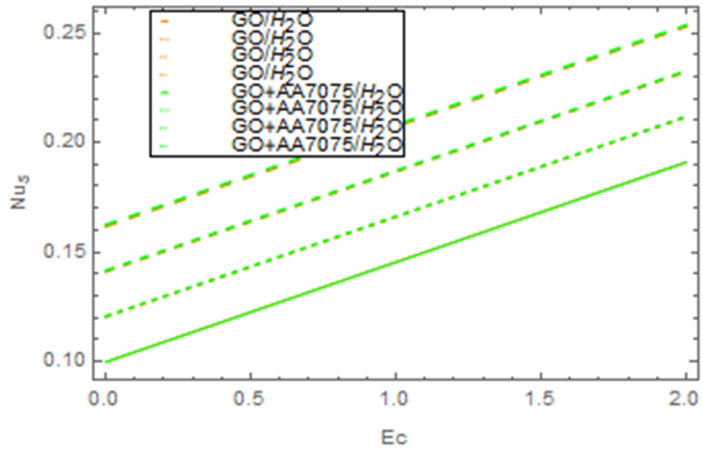

Figure 18: Effect of Ec on Nu_s.

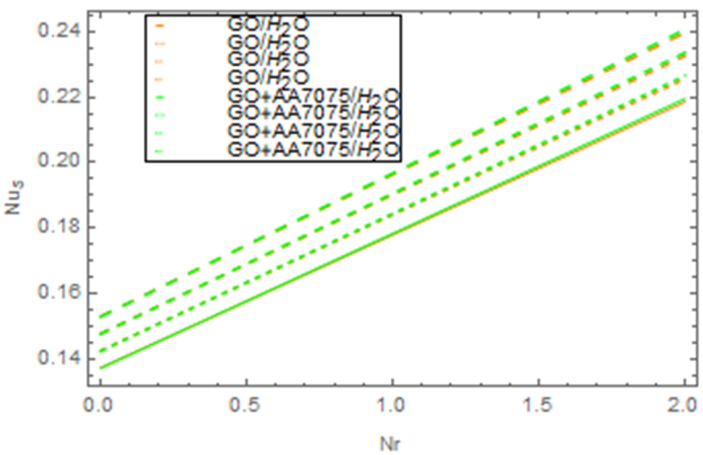

Figure 19: Effect of Nr on Nu_s.

6.4. Comparison and validations

Comparison of some properties of Ree-Eyring Fluids with Newtonian Fluids are shown in Table 6, where Table 7 show the validations of outcome for $C_f(Re_s)^{1/2}$ with previous published results.

Table 9: Comparison of Ree-Eyring Fluids with Newtonian Fluids

Property	**Ree-Eyring Fluids**	**Newtonian Fluids**
Viscosity	Shear-dependent	Uniform
Thermal Boundary Layer	Thinner	Thicker
Heat Transfer	Higher	Lower
Flow Instabilities	Higher	Modest

Table 10: Validations of numerical value of $C_f(Re_s)^{1/2}$ when $M = Nr = Pr = Fr = \Gamma_1 = \Gamma_2 = 0$

γ	Present results	Reddy et al. [5] results
5	1.4196435	1.4196435
10	1.3467243	1.3467243
20	1.3135163	1.3135163
20	1.3028352	1.3028352

7. Conclusion

This work investigates the effects of heat generation and mathematical analysis on the steady magnetized Ree-Erying fluid model?s based on hybrid nanofluid over a curved surface. The study contains a very rich parameter exploration, which includes variations in the Curvature parameter, Schmidt number, Eckert number, thermal radiation parameter or volume fraction, as well as Magnetic parameter, Darcy number and the Prandtl, with the aim of analysing relevant variables such as velocity, temperature, Skin friction and Nusselt profiles, as a result of using similarity transformations to the system of PDEs to transform these into nonlinear ODEs solved analytically. The conclusion is as follows:

- Thermic radiation efficiently increases the heat transfer rate of the flow.
- The thermal boundary layer is regulated by the Biot number and a variable heat source/sink.
- The energy and momentum fields have successfully regulated by the Darcy-Forchheimer parameters.
- PTSC's thermal performance is efficiently improved in the presence of thermal radiation by the Water-GO-AA7075 hybrid nanofluid.
- Heat transmission was improved to raise the Biot number values. This study finds that the flow velocity profile is improved by increasing the values of curvature parameter.
- When magnetic field is increased, the fluid to surface ratio grows and the rate of heat transfer falls.
- The Nusselt number tends to increase with the curvature parameter.
- The increasing behavior of skin friction (Cf_s) for rising values of magnetic parameter (M) for hybrid nanofluid are observed.
- If the Water-GO-AA7075 mixture is utilized instead of the Water-GO combination, the transfer of heat in curved surface can be improved.
- Applications of this study include solar-powered crafts and affordable solar energy generation systems.
- This study investigates the possible applications of the GO-AA7075 hybrid nanofluid for enhancing heat transfer efficiency, showing its ability for solving real-world thermal management problems throughout in many industries.

Parabolic trough solar collectors (PTSC) are widely used for medium-temperature applications, typically operating within a temperature range of 60–400 °C . These systems primarily serve the purpose of heat and power production. In recent years, solar energy has emerged as a significant source of renewable heat energy. One effective approach to enhancing the thermal management systems across various engineering applications is the integration of nanomaterials with conventional heat transfer fluids.

Future work and Limitations

Future research could extend this work by considering three-dimensional flow effects, unsteady flow conditions, and real-time experimental validation to enhance the practical applicability of the proposed model using different geometries. The work can be extended by incorporating different Non-Newtonian flow models and various types of nanofluids. Additionally, it can be expanded by considering different body forces such as MHD, EMHD, and other relevant forces. Optimization techniques can be explored, along with the integration of machine learning approaches and artificial intelligence (AI) to predict optimal parameter values for maximizing heat transfer efficiency. The research can be further validated through numerical simulations and an assessment of the feasibility of using hybrid nanofluids in industrial heat exchangers. Moreover, extending the analysis to transient heat transfer and flow dynamics would provide deeper insights.

Conflicts of Interest

The authors state that they do not have any conflicts of interest.

Data Availability statement

The data that support the study's findings are available upon reasonable request from the corresponding author.

References

1. F Mebarek-Oudina, M Bouselsal, R Djebali, H Vaidya, N Biswas, and K Ramesh. Thermal performance of mgo-swcnt/water hybrid nanofluids in a zigzag walled cavity with differently shaped obstacles. *Modern Physics Letters B*, page 2550163, 2025.

2. Fateh Mebarek-Oudina, G Dharmaiah, JL Rama Prasad, H Vaidya, and Manda Aruna Kumari. Thermal and flow dynamics of magnetohydrodynamic burgers' fluid induced by a stretching cylinder with internal heat generation and absorption. *International Journal of Thermofluids*, 25:100986, 2025.

3. KV Prasad, Fateh Mebarek-Oudina, Hanumesh Vaidya, Rajashekhar Choudhari, Shruthi Karanth, and D Tripathi. Tangent hyperbolic mhd nanoliquids on non-isothermal stretched sheets: Analyzing the impact of transport parameters, variable fluid properties and convective boundary conditions. *Results in Physics*, 66:108008, 2024.

4. Gourab Banerjee, Sourav Sarkar, Achintya Mukhopadhyay, Swarnendu Sen, Pranibesh Mandal, and Suvankar Ganguly. Effect of curvature on heat transfer characteristics for jet impingement cooling of a moving surface. In *Conference on Fluid Mechanics and Fluid Power*, pages 415–420. Springer, 2021.

5. B Ould Said, F Mebarek-Oudina, and MA Medebber. Magneto-hydro-convective nanofluid flow in porous square enclosure. *Frontiers in Heat and Mass Transfer*, 22(5):1343–1360, 2024.

6. Jawad Raza, F Mebarek-Oudina, Haider Ali, and IE Sarris. Slip effects on casson nanofluid over a stretching sheet with activation energy: Rsm analysis. *Frontiers in Heat and Mass Transfer*, 22(4):1017–1041, 2024.

7. M Anil Kumar, F Mebarek-Oudina, P Mangathai, NA Shah, Ch Vijayabhaskar, N Venkatesh, and Y Fouad. The impact of soret dufour and radiation on the laminar flow of a rotating liquid past a porous plate via chemical reaction. *Modern Physics Letters B*, 39(10):2450458, 2025.

8. Joe S Coventry. Performance of a concentrating photovoltaic/thermal solar collector. *Solar energy*, 78(2):211–222, 2005.

9. Vasudeva Reddy Minnam Reddy, M Girinath Reddy, PA Dinesh, and N Sandeep. Enhanced heat transfer efficiency of ptsc using hydromagnetic cross nanofluid: a hydrogen energy application. *International Journal of Hydrogen Energy*, 47(46):20254–20264, 2022.

10. Hussein A Mohammed, Hari B Vuthaluru, and Shaomin Liu. Heat transfer augmentation of parabolic trough solar collector receiver's tube using hybrid nanofluids and conical turbulators. *Journal of the Taiwan Institute of Chemical Engineers*, 125:215–242, 2021.

11. Asim Aziz, Wasim Jamshed, Taha Aziz, Haitham MS Bahaidarah, and Khalil Ur Rehman. Entropy analysis of powell–eyring hybrid nanofluid including effect of linear thermal radiation and viscous dissipation. *Journal of Thermal Analysis and Calorimetry*, 143(2):1331–1343, 2021.

12. Umair Rashid, Dumitru Baleanu, Azhar Iqbal, and Muhammd Abbas. Shape effect of nanosize particles on magneto-hydrodynamic nanofluid flow and heat transfer over a stretching sheet with entropy generation. *Entropy*, 22(10):1171, 2020.

13. S Kadri, K Djermane, E Bourbaba, M Elmir, and R Mehdaoui. Numerical investigation of natural convection in an inclined wavy solar collector containing a nanofluid. *The International Journal of Multiphysics*, 14(2):115–128, 2020.

14. Abdulwahab A Alnaqi, Jalal Alsarraf, and Abdullah AAA Al-Rashed. Numerical investigation of hydrothermal efficiency of a parabolic dish solar collector filled with oil based hybrid nanofluid. *Journal of the Taiwan Institute of Chemical Engineers*, 124:238–257, 2021.

15. Farooq Ahmad, Sohaib Abdal, Hela Ayed, Sajjad Hussain, Suleman Salim, and A Othman Almatroud. The improved thermal efficiency of maxwell hybrid nanofluid comprising of graphene oxide plus silver/kerosene oil over stretching sheet. *Case Studies in Thermal Engineering*, 27:101257, 2021.

16. Choi Sus. Enhancing thermal conductivity of fluids with nanoparticles, developments and applications of non-newtonian flows. *ASME, FED, MD, 1995*, 231:99–I05, 1995.

17. Hossein Chaji, Yahya Ajabshirchi, Esmaeil Esmaeilzadeh, S Zeinali Heris, Mahdi Hedayatizadeh, and Mostafa Kahani. Experimental study on thermal efficiency of flat plate solar collector using tio2/water nanofluid. *Modern Applied Science*, 7(10):60–69, 2013.

18. Seyed Ebrahim Ghasemi, AHANGAR GH R MEHDIZADEH, et al. Numerical analysis of performance of solar parabolic trough collector with cu-water nanofluid. 2014.

19. Morteza Ghanbarpour and Rahmatollah Khodabandeh. Entropy generation analysis of cylindrical heat pipe using nanofluid. *Thermochimica Acta*, 610:37–46, 2015.

20. Geng Liu, YA Cengel, and RH Turner. Exergy analysis of a solar heating system. *Journal of solar energy engineering*, 117(3):249–251, 1995.

21. Wasim Jamshed, Kottakkaran Sooppy Nisar, Rabha W Ibrahim, Faisal Shahzad, and Mohamed R Eid. Thermal expansion optimization in solar aircraft using tangent hyperbolic hybrid nanofluid: A solar thermal application. *Journal of Materials Research and Technology*, 14:985–1006, 2021.

22. Yaseen H Mahmood, Adnan M Khalid, and Abdulsalam S Baqi. Theoretical efficiency and practicality of the solar trough collector/tikrit-iraq. *NeuroQuantology*, 19(5):18–24, 2021.

23. Muhammad Ijaz Khan, Sohail Ahmad Khan, Tasawar Hayat, Muhammad Faisal Javed, and Muhammad Waqas. Entropy generation in radiative flow of ree-eyring fluid due to due rotating disks. *International Journal of Numerical Methods for Heat & Fluid Flow*, 30(4):1839–1865, 2020.

24. V Puneeth, Farhan Ali, M Riaz Khan, M Shoaib Anwar, and N Ameer Ahammad. Theoretical analysis of the thermal characteristics of ree–eyring nanofluid flowing past a stretching sheet due to bioconvection. *Biomass Conversion and Biorefinery*, 14(7):8649–8660, 2024.

25. NF Okechi, M Jalil, and S Asghar. Flow of viscous fluid along an exponentially stretching curved surface. *Results in Physics*, 7:2851–2854, 2017.

26. Tayeb Fahim, Samir Laouedj, Aissa Abderrahmane, Zied Driss, El Sayed Mohamed Tag-ElDin, Kamel Guedri, and Obai Younis. Numerical study of perforated obstacles effects on the performance of solar parabolic trough collector. *Frontiers in Chemistry*, 10:1089080, 2023.

27. Tayeb Fahim, Samir Laouedj, Aissa Abderrahmane, Sorour Alotaibi, Obai Younis, and Hafiz Muhammad Ali. Heat transfer enhancement in parabolic through solar receiver: a three-dimensional numerical investigation. *Nanomaterials*, 12(3):419, 2022.

Hamayat Ullah,

Department of Mathematical Sciences,

University of Lakki Marwat, Lakki Marwat 28420, KPK, Pakistan.

E-mail address: hamayatullahmath17@gmail.com

and

Zahir Shah,

Department of Mathematical Sciences,

University of Lakki Marwat, Lakki Marwat 28420, KPK, Pakistan.

E-mail address: zahir@ulm.edu.pk

and

Waris Khan,

Department of Mathematics, Hazara University of science and Technology, Hazara, Pakistan

E-mail address: wariskhan758@yahoo.com

and

Maria Alina Fălădău,
Faculty of Engineering,
Lucian Blaga University of Sibiu, 550024 Sibiu, Romania.
E-mail address: alina.gligor@ulbsibiu.ro

and

Aseel Smerat,
Faculty of Educational Sciences,
Al-Ahliyya Amman University, Amman, 19328, Jordan.
Department of Biosciences, Saveetha School of Engineering,
Saveetha Institute of Medical and Technical Sciences, Chennai, 602105, India.
E-mail address: smerat.2020@gmail.com

and

Rashid Jan,
Department of Mathematics, College of Science, Qassim University, Buraydah, 51452, Saudi Arabia
E-mail address: r.jehan@qu.edu.sa